

Quasimolecular $J_{\text{tet}} = 3/2$ moments in the cluster Mott insulator GaTa_4Se_8

M. Magnaterra,¹ J. Attig,² L. Peterlini,² M. Hermanns,³ M. H. Upton,⁴ Jungho Kim,⁴ L. Prodan,⁵ V. Tsurkan,^{5,6} I. Kézsmárki,⁵ P.H.M. van Loosdrecht,¹ and M. Grüninger¹

¹Institute of Physics II, University of Cologne, 50937 Cologne, Germany

²Institute for Theoretical Physics, University of Cologne, 50937 Cologne, Germany

³Department of Physics, Stockholm University, AlbaNova University Center, SE-106 91 Stockholm, Sweden

⁴Advanced Photon Source, Argonne National Laboratory, Argonne, Illinois 60439, USA

⁵Experimental Physics V, Center for Electronic Correlations and Magnetism, University of Augsburg, Germany

⁶Institute of Applied Physics, Moldova State University, MD 2028, Chisinau, R. of Moldova

(Dated: September 21, 2023)

Quasimolecular orbitals in cluster Mott insulators provide a route to tailor exchange interactions, which may yield novel quantum phases of matter. We demonstrate the cluster Mott character of the lacunar spinel GaTa_4Se_8 using resonant inelastic x-ray scattering (RIXS) at the Ta L_3 edge. Electrons are fully delocalized over Ta_4 tetrahedra, forming quasimolecular $J_{\text{tet}} = 3/2$ moments. The modulation of the RIXS intensity as function of the transferred momentum \mathbf{q} allows us to determine the cluster wavefunction, which depends on competing intracluster hopping terms that mix states with different character. This mixed wavefunction is decisive for the macroscopic properties since it affects intercluster hopping and exchange interactions and furthermore renormalizes the effective spin-orbit coupling constant. The versatile wavefunction, tunable via intracluster hopping, opens a new perspective on the large family of lacunar spinels and cluster Mott insulators in general.

With strong spin-orbit coupling, novel forms of quantum magnetism may emerge from unconventional magnetic moments that exhibit exotic exchange couplings. The Kitaev spin liquid is a prominent example [1, 2]. Bond-directional Kitaev exchange has been realized in, e.g., $5d^5$ honeycomb iridates with spin-orbit-entangled $j = 1/2$ moments [3–7]. Another intriguing case is given by $5d^1$ $j = 3/2$ moments on an *fcc* lattice, e.g., in double perovskites. These moments experience bond-dependent multipolar interactions, giving rise to a rich phase diagram that includes multipolar order and a chiral quantum spin liquid with Majorana fermion excitations [8–11].

Exchange-coupled local moments exist in Mott insulators, where electrons are localized on individual sites. A new flavor is offered by cluster Mott insulators, which can be viewed as the electronic equivalent of a molecular crystal [12–17]. In these, electrons occupy quasimolecular orbitals that are delocalized over a cluster, e.g., a dimer or trimer, while intercluster charge fluctuations are suppressed by Coulomb repulsion. The emerging quasimolecular magnetic moments are the fundamental units determining the macroscopic low-energy properties. Importantly, the character of these moments can be tuned by internal degrees of freedom. One example is an Ir_2O_9 dimer with three holes as in the spin-liquid candidate $\text{Ba}_3\text{InIr}_2\text{O}_9$ [18]. With increasing intradimer hopping, the dimer moments change from $J_{\text{dim}} = 1/2$ to $3/2$ [19, 20]. In general, the quasimolecular wavefunction depends on competing intracluster hopping terms and is highly sensitive to the cluster shape. The ability to tune intracluster hopping via external or chemical pressure offers the promising perspective to tailor the moments and thereby the character and symmetry of intercluster exchange interactions with the aim to realize novel magnetic quantum phases of matter.

We focus on the transition-metal M_4 tetrahedra in the large family of lacunar spinels AM_4X_8 ($M = \text{V, Ti, Mo, Nb, Ta}$; $A = \text{Ga, Ge, Al}$; $X = \text{S, Se, Te}$) [12, 21–24], see Fig. 1. With one electron in a quasimolecular t_2 orbital, ideal $J_{\text{tet}} = 3/2$ moments forming an *fcc* lattice have been claimed to be realized

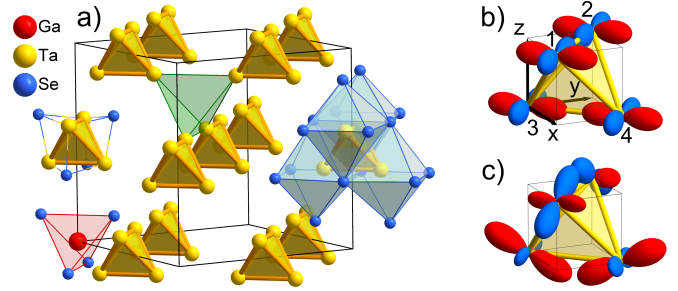


FIG. 1. a) Simplified sketch of cubic GaTa_4Se_8 [23]. Not all Ga and Se ions are shown. The structure corresponds to a NaCl-like lattice of tetrahedral $(\text{GaSe}_4)^{-5}$ (red) and heterocubane $(\text{Ta}_4\text{Se}_4)^{+5}$ units. Tetrahedral Ta_4 clusters (yellow) arise from edge-sharing TaSe_6 octahedra (blue) and form an *fcc* lattice. The intracluster Ta-Ta distance $d = 3.0 \text{ \AA}$ is much shorter than the intercluster one (4.3 \AA , edges of green tetrahedron). b) Bonding quasimolecular xy_b orbital, see Eq. (1). c) $t_2(xy)$ orbital with sizable antibonding character, see Eq. (3) for $\alpha = 2$.

in $5d$ GaTa_4Se_8 [25, 26]. Remarkably, a cluster Mott character has also been proposed, mainly based on band-structure calculations, for the $4d$ and even the $3d$ compounds, where smaller hopping competes with larger on-site Coulomb repulsion U [12, 13, 24, 25, 27–32]. However, a direct experimental proof of quasimolecular electronic states in the lacunar spinels is still lacking. Such a quasimolecular character is particularly intriguing in the light of the complex phase diagrams of the lacunar spinels, which include multiple multiferroic and skyrmion-lattice phases with, e.g., Néel-type skyrmions carrying electric polarization [33–36], (anti-)ferroelectric states with peculiar domain architectures [37–39], and magnetism tied to polar domain walls [40]. The $5d$ Ta compounds host a pressure-induced insulator-to-metal transition followed by topological superconductivity [13, 41–43] and an avalanche-type dielectric breakdown of the Mott gap [44].

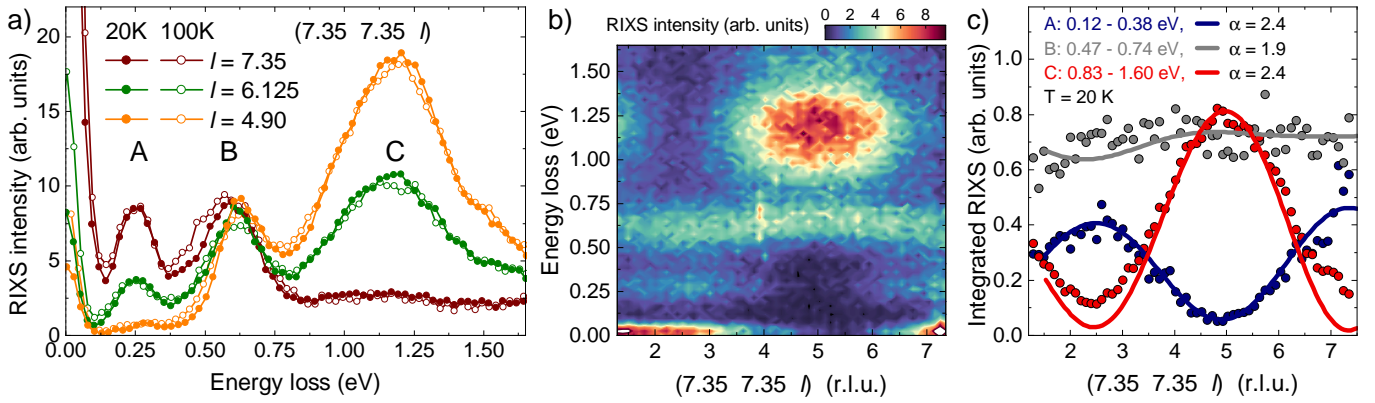


FIG. 2. RIXS data of GaTa_4Se_8 along $(7.35 \ 7.35 \ l)$. a) Spectra acquired at 20 and 100 K show the three peaks A, B, and C. Changing \mathbf{q} strongly affects the intensity. b) Color map of the RIXS intensity at 20 K. Independent of the cluster modulation, the elastic line is suppressed around $l = 5.4$ due to a scattering angle 2θ close to 90° . c) Integrated intensity of peaks A, B and C. Integration intervals are given in the panel. Peaks A and C show dominant $\sin^2(\pi l/4.9)$ and $\cos^2(\pi l/4.9)$ behavior, respectively. Solid lines: Results of the single-particle model.

Here, we address the cluster wavefunction, which is the essential starting point for a comprehensive understanding of the lacunar spinels. We study GaTa_4Se_8 via resonant inelastic x-ray scattering (RIXS) at the Ta L_3 edge. RIXS directly probes the quasimolecular nature of, e.g., intra- t_2^1 excitations and pinpoints that the electrons are fully delocalized over a Ta_4 tetrahedron while correlations hardly affect the t_2^1 manifold. We find that the quasimolecular $J_{\text{tet}} = 3/2$ wavefunction deviates from the idealized case assumed previously [25, 26], since competing intracluster hopping terms mutually mix the corresponding bonding and antibonding orbitals. In GaTa_4Se_8 , this mixing reduces the effective spin-orbit coupling constant ζ_{eff} by roughly $1/3$. Arising from strong hopping, the mixing is not a small perturbation and can be expected to affect the exchange interactions. Based on this mixing, the cluster wavefunction is sensitive to structural changes due to, e.g., external pressure or chemical substitution, which provides a new perspective on the entire family of lacunar spinels.

The delocalization of electrons over a cluster yields a characteristic modulation of the RIXS intensity $I(\mathbf{q})$ as function of the transferred momentum \mathbf{q} . This modulation reflects the dynamical structure factor $S(\mathbf{q}, \omega)$ and reveals the character and symmetry of electronic states. For a dimer, RIXS can be described as an inelastic version of Young’s double-slit experiment [45]. The corresponding sinusoidal interference pattern has been observed recently in $\text{Ba}_3\text{CeIr}_2\text{O}_9$ and related dimer compounds [20, 46, 47]. Stuningly, a sinusoidal intensity modulation has also been found in the Kitaev material Na_2IrO_3 where it unravels the bond-directional nearest-neighbor character of the magnetic excitations [7, 48]. Careful consideration of these interference effects is a prerequisite for the analysis of RIXS in cluster Mott insulators and provides a powerful tool to address the electronic states of GaTa_4Se_8 .

Single crystals of GaTa_4Se_8 were grown by chemical vapor transport [49]. At 300 K, GaTa_4Se_8 shows the noncentrosymmetric cubic space group $F\bar{4}3m$ with lattice constant $a = 10.382 \text{ \AA}$ [23], see Fig. 1. The short intratetrahedral Ta-Ta distance $d = 3.0 \text{ \AA}$ suggests a quasimolecular character. The optical conductivity characterizes the lacunar spinels as

narrow-gap insulators and reveals a Mott gap of 0.12 eV in GaTa_4Se_8 [44, 50, 51]. Experimental results for the magnetic moment per Ta_4 cluster yield 0.7-1.2 μ_B [23, 52–54]. The magnetostructural transition at $T_{\text{ms}} = 53 \text{ K}$ is accompanied by a strong drop in the magnetic susceptibility [52, 54, 55], but the crystal symmetry at low temperature is still under debate [24, 54–56]. We first focus on cubic symmetry and then address the effect of distortions.

We measured RIXS at the Ta L_3 edge at Sector 27 at the Advanced Photon Source [57]. The incident energy 9.879 keV resonantly enhances excitations within the Ta t_{2g} orbitals [26]. We studied a (111) surface with the (110) and (001) directions in the horizontal scattering plane, using incident π polarization. An energy resolution $\Delta E = 76 \text{ meV}$ was achieved using a Si(440) four-bounce monochromator and a $R = 2 \text{ m}$ Si(066) spherical diced crystal analyzer. We subtracted a background intensity that was determined by averaging over a range of negative energy loss. All spectra have been corrected for geometrical self-absorption [58]. We express \mathbf{q} in reciprocal lattice units (r.l.u.). The \mathbf{q} resolution equals $\Delta\mathbf{q} = (0.1 \ 0.1 \ 0.3)$.

The RIXS spectra of GaTa_4Se_8 show three peaks A, B, and C at about 0.25, 0.62, and 1.2 eV, see Fig. 2a). The peak energies hardly show any dispersion but the intensity strongly depends on \mathbf{q} , in agreement with the data of Jeong *et al.* [26]. This is a first indication of the local, quasimolecular character of the electronic states. For the peak assignment, we address the electronic structure of a single Ta_4 tetrahedron, starting with a non-interacting picture in the undistorted cubic case. Note that the RIXS data at 20 K and 100 K, i.e., above and below the structural transition at 53 K, are very similar.

Due to the large cubic crystal-field splitting $10 Dq \approx 3 \text{ eV}$ [26], it is sufficient to consider the Ta t_{2g} states. Direct σ -type hopping $t_\sigma \equiv t_{dd\sigma}$ of order 1 eV [25] yields bonding (b) and antibonding (ab) states at $\pm t_\sigma$. Adding π -type hopping $t_\pi \equiv t_{dd\pi}$ results in the quasimolecular orbitals a_1 , e , and t_2 at low energy and further states at high energy, see Fig. 3a). With 7 electrons per Ta_4 cluster, the ground state shows fully occupied a_1 and e orbitals plus a single electron in the t_2 states, $a_1^2 e^4 t_2^1$. The three t_2 orbitals are central to our discussion. Due

to t_π , they are mixtures of bonding and antibonding states of t_σ , see Fig. 3a). We will show the relevance of this mixture below but first follow the typical assumption where only the bonding ones are considered. This yields (cf. Fig. 1b)

$$xy_b = (xy_1 + xy_2 + xy_3 + xy_4) / 2 \quad (1)$$

and equivalent for yz_b and xz_b , where $i = 1-4$ denotes the Ta sites. Projecting spin-orbit coupling ζ onto the subspace of these t_2^1 states yields a cluster Hamiltonian that is fully equivalent to the single-site case [3], see *Supplementary Information* [59]. It shows a $J_{\text{tet}} = 3/2$ ground state and a $J_{\text{tet}} = 1/2$ excited state at 1.5ζ [25]. The latter, the so-called spin-orbit exciton, corresponds to peak A, while peaks B and C in this non-interacting scenario are assigned to excitations from e to J_{tet} states, i.e., from $e^4 t_2^1$ to $e^3 t_2^2$, see Fig. 3a).

This peak assignment is supported by quantum chemistry calculations [53] and is confirmed by the characteristic \mathbf{q} dependence of the RIXS intensity. Figure 2b) is a color plot for energies up to 1.6 eV, while Fig. 2c) shows the integrated RIXS intensity of peaks A, B, and C for \mathbf{q} along (7.35 7.35 l) together with results of a single-particle calculation (see below). Peak B hardly depends on \mathbf{q} , while A and C show a pronounced $\sin^2(\pi l/4.9)$ and $\cos^2(\pi l/4.9)$ behavior, respectively, reflecting the different symmetries of the corresponding states. The period $l_0 = 4.9$ points to a Ta-Ta distance of $a/4.9 \approx 2.12 \text{ \AA}$ that agrees with the c -axis projection $d/\sqrt{2} \approx 2.12 \text{ \AA}$ of the intratetrahedral Ta-Ta distance d . Spectra for $l = l_0$ and $l = 1.5l_0 = 7.35$ correspond to extrema of the intensity modulation, cf. Fig. 2a).

The dominant $\sin^2(\pi l/4.9)$ behavior of peak A is a clear fingerprint of the quasimolecular intra- t_2^1 spin-orbit exciton. In general, the RIXS intensity for an excitation from the ground state $|0\rangle$ to a final state $|f\rangle$ is described by [60, 61]

$$I_f(\mathbf{q}, \omega) = \left| \langle f | \sum_{\gamma} e^{i\mathbf{q}\cdot\mathbf{R}_\gamma} D_\gamma^\dagger D_\gamma | 0 \rangle \right|^2 \delta(\hbar\omega - E_f) \quad (2)$$

where E_f denotes the excitation energy and D_γ (D_γ^\dagger) is the local dipole operator for resonant scattering at the Ta site \mathbf{R}_γ . This coherent sum of local scattering processes is running over all \mathbf{R}_γ from which the final state $|f\rangle$ can be reached. For the quasimolecular states in GaTa_4Se_8 , this refers to the four Ta sites of a tetrahedron. For \mathbf{q} along (7.35 7.35 l), the physics is particularly simple if we stick to the contribution of bonding states to the quasimolecular t_2 orbitals, see Fig. 3a), i.e., we employ Eq. (1) and the associated J_{tet} states for spin-orbit coupling within the t_2 states, as discussed above. In this case, $I_{B/C}(l) \propto \cos^2(\pi l/4.9)$ for all excitations from e to t_2 , while only the spin-orbit exciton is expected to show $I_A(l) \propto \sin^2(\pi l/4.9)$, see dashed lines in Fig. 4a)-c). This firmly supports our interpretation of peak A.

Our central goal is to determine the cluster wavefunction. Thus far, we considered only the bonding contributions to the t_2 orbitals, see Eq. (1), a common approximation [25, 26]. In this simple bonding picture, $I_C(l)$ describes the overall behavior of peak C but $I_B(l)$ does not explain the nearly \mathbf{q} -independent intensity of peak B. Furthermore, this approximation predicts the spin-orbit exciton at 1.5ζ , as for a single site, which is hard to reconcile with the energy of peak

A at 0.25 eV. The equivalent excitation for weakly interacting Ta $5d^1$ ions has been observed in RIXS on Rb_2TaCl_6 at 0.4 eV [63], resulting in $\zeta \approx 0.27$ eV. Compared to 0.4 eV, the energy of peak A is about 40 % smaller. As shown below, these critical issues are resolved by considering the admixture of antibonding character to the t_2 orbitals. With the intracluster hoppings t_σ and t_π , the eigenstate $t_2(xy)$ of the hopping Hamiltonian reads

$$t_2(xy) = [xy_b - (yz_{ab} - xz_{ab})/\alpha] / \sqrt{1 + (2/\alpha^2)} \quad (3)$$

with the antibonding orbitals $yz_{ab} = (yz_1 - yz_2 + yz_3 - yz_4)/2$ and $xz_{ab} = (xz_1 - xz_2 - xz_3 + xz_4)/2$. The approximation of Eq. (1) corresponds to $\alpha = \infty$. The mixing coefficient reads

$$\alpha = |t_\sigma/t_\pi| - 3/2 + \sqrt{(|t_\sigma/t_\pi| - 3/2)^2 + 2}. \quad (4)$$

Projecting spin-orbit coupling onto this t_2^1 subspace yields the same cluster Hamiltonian as above [59] but with renormalized coupling constant $\zeta_{\text{eff}} = \zeta \cdot (\alpha^2 - 1) / (\alpha^2 + 2)$. Accordingly, the peak assignment of Fig. 3a) is still valid but α renormalizes in particular the energy of peak A, cf. Fig. 3b), and changes the character of the quasimolecular J_{tet} states. Using Harrison's empirical d dependence of the Slater-Koster parameters [64], we find $|t_\sigma/t_\pi| = 1.5|V_{dd\sigma}/V_{dd\pi}| \approx 2.8$. This yields a first estimate $\alpha \approx 3.2$. Taking into account hopping t_{Se} via the Se ligands reduces α , for instance to $\alpha \approx 2$ for $t_{\text{Se}} \approx t_\pi$. The $t_2(xy)$ orbital for $\alpha = 2$ is depicted in Fig. 1c).

Experimentally, the \mathbf{q} -dependent RIXS intensity is the ideal tool to determine the mixing coefficient α . Via the matrix elements in Eq. (2), RIXS is directly sensitive to the quasimolecular wavefunction and hence to the admixture of antibonding orbitals. We calculated the RIXS response in the single-particle picture for spin-orbit coupling within the t_2 states, taking into account polarization selection rules. Results for the normalized RIXS intensities of peaks A, B, and C along (7.35 7.35 l) and two further \mathbf{q} directions are plotted in Fig. 4. Along ($k+0.15$ k 4.8), the dominant term for

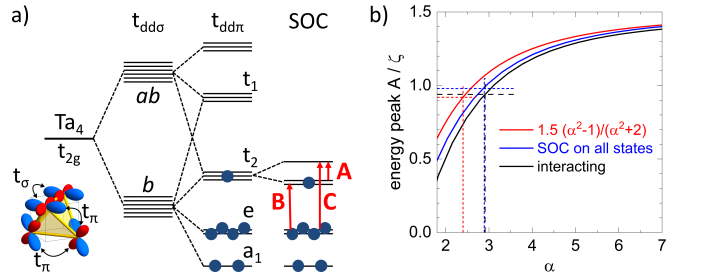


FIG. 3. a) Single-particle energy levels of a Ta_4 tetrahedron. Intracluster hopping (see bottom left) yields quasimolecular orbitals and an $a_1^2 e^4 t_2^1$ ground state. Because of t_π , the t_2 orbitals show contributions of bonding (b) and antibonding (ab) states of t_σ . Spin-orbit coupling within the t_2^1 states forms a $J_{\text{tet}} = 3/2$ ground state. A, B, and C refer to the RIXS peaks, see Fig. 2. b) The admixture of antibonding character renormalizes the energy of peak A, see Eq. (3). Red (blue): single-particle result for spin-orbit coupling within t_2 (all) states. Black: many-body cluster calculation using Quany [62], see *Supplementary Information* [59]. Dashed lines: value of α derived from the \mathbf{q} dependence and corresponding excitation energy.

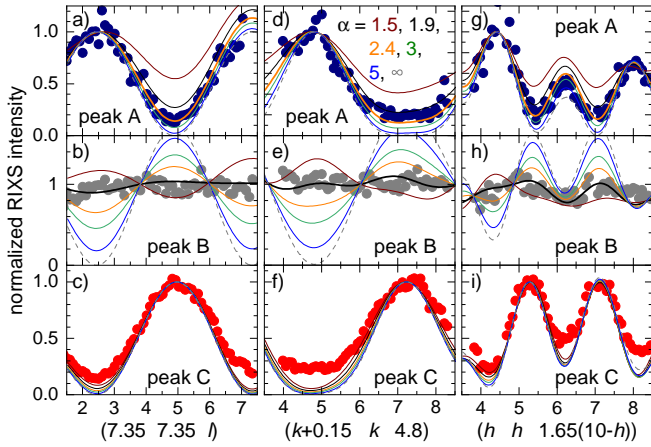


FIG. 4. Normalized RIXS intensity (symbols) along three \mathbf{q} directions for peaks A, B and C with integration ranges as in Fig. 2. Lines: Results of the single-particle model for spin-orbit coupling within the t_2 states. Note that α is the only free parameter. For peaks A and B, best agreement is obtained for $\alpha = 2.4 \pm 0.3$ and $1.8-1.9$, respectively. Dashed: Result for $\alpha = \infty$, neglecting antibonding states.

peak A is $\cos^4(\pi k/4.9)$ while a more complex behavior is observed along $(h \ h \ 1.65(10-h))$. The single-particle picture captures the behavior of all three peaks surprisingly well. We emphasize that α is the only free parameter in Fig. 4, reflecting the dependence of the wavefunction on t_σ and t_π . These results unambiguously establish the quasimolecular cluster-Mott character of GaTa_4Se_8 and that the admixture of antibonding character is sizable, i.e., $1/\alpha$ is not small.

The single-particle picture is expected to work particularly well for the intra- t_2^1 excitation of the spin-orbit exciton, peak A. Peaks B and C with $e^3 t_2^2$ final states will be more sensitive to interactions. Peak C is the least sensitive to α . The single-particle model reproduces the overall \mathbf{q} dependence but fails to describe the minima quantitatively. To some extent, this may reflect a possible background contribution of excitations across the Mott gap at high energies. In contrast, peak B is highly sensitive to α . Its nearly constant behavior as function of \mathbf{q} is reproduced in a narrow window $\alpha = 1.8-1.9$. For peak A, excellent agreement is found for $\alpha = 2.4 \pm 0.3$.

These results for α fall in the range predicted above based on Harrison's rules. The precise value depends on details of the model concerning the range of spin-orbit coupling, distortions, sub-leading hopping terms, and correlations. Above, spin-orbit coupling was projected onto t_2 orbitals only. If we instead consider all orbitals, in particular including e and t_1 (see Fig. 3a), peak A is best described for $\alpha = 2.9 \pm 0.4$. Furthermore, we discussed regular tetrahedra but the symmetry is lower than cubic below $T_{ms} = 53$ K. Recent x-ray and neutron results on the pair distribution function [56] point to dynamical local distortions up to temperatures far above T_{ms} . For trigonally distorted tetrahedra, we find that RIXS is sensitive to the distortion if a single orientation can be studied while the average over different orientations is very close to the cubic case, see *Supplementary Information* [59]. The latter applies to both 20 and 100 K and validates our approach.

However, a distortion of the tetrahedra with less than trigonal symmetry affects the value of α for which peak B is nearly independent of \mathbf{q} , see *Supplementary Information* [59]. Note that different results were reported for the crystal symmetry at low temperature [24, 54–56], impeding an even more precise determination of α at present.

In a cluster Mott insulator, electron-electron interactions suppress intercluster charge transport. Within a cluster, correlations compete with dominant hopping that delocalizes the electrons in quasimolecular orbitals. To study the effect on the RIXS response, we performed many-body calculations for a single tetrahedron using Quany [62], see *Supplementary Information* [59]. Interactions yield a fanning out of the $a_1^2 e^3 t_2^2$ energy levels that is relevant to explaining the width of peak C and the energies of B and C, supporting our peak assignment. For peak A, we find that electron-electron interactions have only a minor effect on both the energy and the \mathbf{q} -dependent intensity, in particular for comparison with the case where spin-orbit coupling is not restricted to t_2 , see *Supplementary Information* [59]. The many-body calculations thus support the overall picture of the single-particle model.

The renormalized energy of the spin-orbit exciton, peak A, provides an independent means to test our results for α . Figure 3b) shows the single-particle result for spin-orbit coupling within t_2 , $E_{SO} = 1.5\zeta_{\text{eff}} = 1.5\zeta(\alpha^2 - 1)/(\alpha^2 + 2)$. For comparison, the excitation energy is also given for spin-orbit coupling acting on all states and for the many-body cluster calculation. For the latter we change α by changing t_σ , cf. Eq. (4), with all other parameters fixed. The overall behavior is very similar. For all three cases, the dashed lines denote the value of α that best describes the \mathbf{q} dependence. This yields an excitation energy of $0.9-1.0\zeta$ and hence $\zeta \approx 0.27-0.30$ eV, in very good agreement with both quantum chemistry calculations [53] and the value 0.27 eV reported for $5d^1$ Rb_2TaCl_6 [63].

In conclusion, our results establish GaTa_4Se_8 as a fascinating example of a cluster Mott insulator. The valence electrons are fully delocalized over a Ta_4 tetrahedron, while intercluster charge fluctuations are suppressed. A thorough analysis of the modulated RIXS intensity $I(\mathbf{q})$ reveals the quasimolecular wavefunction, which is the essential starting point for exploring the physics of cluster Mott insulators. The spin-orbit exciton, an excitation within the t_2^1 manifold, is particularly well described in a single-particle scenario that is coined by competing hopping terms, t_σ and t_π . This competition shapes the wavefunction, renormalizes the effective spin-orbit coupling constant by roughly $1/3$, and hence affects the nature of the quasimolecular magnetic moment. We expect that this is decisive for intercluster exchange coupling, calling for future theoretical investigations. In general, the mixing coefficient α also depends on $t_{ad\delta}$ and on the indirect hopping via ligands. Therefore, it is reasonable to assume that α can be tuned in the lacunar spinels by external pressure and chemical substitution, and one may speculate that even temperature may tip the balance in certain cases. Our results on the quasimolecular character, the particular role of antibonding states, and the tunability of the wavefunction are relevant for many of the open questions on the large family of lacunar spinels.

ACKNOWLEDGMENTS

We thank D. I. Khomskii and J. van den Brink for fruitful discussions and A. Revelli for experimental support. We gratefully acknowledge the Advanced Photon Source (APS) for providing beam time and technical support. APS is a U.S. Department of Energy (DOE) Office of Science user facility operated for the DOE Office of Science by Argonne National Laboratory under Contract No. DE-AC02-

06CH11357. Furthermore, we acknowledge funding from the Deutsche Forschungsgemeinschaft (DFG, German Research Foundation) via Project numbers 277146847 (CRC 1238, projects B03, C03), 492547816 (TRR 360), and 437124857 (KE 2370/3-1). V.T. acknowledges the support via project ANCD 20.80009.5007.19 (Moldova). M.H. acknowledges partial funding by the Knut and Alice Wallenberg Foundation as part of the Wallenberg Academy Fellows project.

-
- [1] A. Kitaev, Anyons in an exactly solved model and beyond, *Annals of Physics* **321**, 2 (2006).
- [2] M. Hermanns, I. Kimchi, and J. Knolle, Physics of the Kitaev Model: Fractionalization, Dynamic Correlations, and Material Connections, *Annual Review of Condensed Matter Physics* **9**, 17 (2018).
- [3] G. Jackeli and G. Khaliullin, Mott Insulators in the Strong Spin-Orbit Coupling Limit: From Heisenberg to a Quantum Compass and Kitaev Models, *Phys. Rev. Lett.* **102**, 017205 (2009).
- [4] J. G. Rau, E. K.-H. Lee, and H.-Y. Kee, Spin-Orbit Physics Giving Rise to Novel Phases in Correlated Systems: Iridates and Related Materials, *Annu. Rev. Condens. Matter Phys.* **7**, 195 (2016).
- [5] S. Trebst and C. Hickey, Kitaev materials, *Phys. Rep.* **950**, 1 (2022).
- [6] S. H. Chun, J.-W. Kim, J. Kim, H. Zheng, C. C. Stoumpos, C. D. Malliakas, J. F. Mitchell, K. Mehlawat, Y. Singh, Y. Choi, T. Gog, A. Al-Zein, M. Moretti Sala, M. Krisch, J. Chaloupka, G. Jackeli, G. Khaliullin, and B. J. Kim, Direct evidence for dominant bond-directional interactions in a honeycomb lattice iridate Na_2IrO_3 , *Nat. Phys.* **11**, 462 (2015).
- [7] M. Magnaterra, K. Hopfer, C. J. Sahle, M. Moretti Sala, G. Monaco, J. Attig, C. Hickey, I.-M. Pietsch, F. Breitner, P. Gegenwart, M. H. Upton, J. Kim, S. Trebst, P. H. M. van Loosdrecht, J. van den Brink, and M. Grüninger, RIXS observation of bond-directional nearest-neighbor excitations in the Kitaev material Na_2IrO_3 , arXiv: 2301.08340 (2023).
- [8] G. Chen, R. Pereira, and L. Balents, Exotic phases induced by strong spin-orbit coupling in ordered double perovskites, *Phys. Rev. B* **82**, 174440 (2010).
- [9] W. M. H. Natori, E. C. Andrade, E. Miranda, and R. G. Pereira, Chiral spin-orbital liquids with nodal lines, *Phys. Rev. Lett.* **117**, 017204 (2016).
- [10] J. Romhányi, L. Balents, and G. Jackeli, Spin-orbit dimers and noncollinear phases in d^1 cubic double perovskites, *Phys. Rev. Lett.* **118**, 217202 (2017).
- [11] A. Mansouri Tehrani, J.-R. Soh, J. Pásztorová, M. E. Merkel, I. Živković, H. M. Rønnow, and N. A. Spaldin, Charge multipole correlations and order in Cs_2TaCl_6 , *Phys. Rev. Res.* **5**, L012010 (2023).
- [12] R. Pocha, D. Johrendt, and R. Pöttgen, Electronic and Structural Instabilities in GaV_4S_8 and GaMo_4S_8 , *Chem. Mater.* **12**, 2882 (2000).
- [13] M. M. Abd-Elmeguid, B. Ni, D. I. Khomskii, R. Pocha, D. Johrendt, X. Wang, and K. Syassen, Transition from Mott Insulator to Superconductor in GaNb_4Se_8 and GaTa_4Se_8 under High Pressure, *Phys. Rev. Lett.* **93**, 126403 (2004).
- [14] J. P. Sheckelton, J. R. Neilson, D. G. Soltan, and T. M. McQueen, Possible valence-bond condensation in the frustrated cluster magnet $\text{LiZn}_2\text{Mo}_3\text{O}_8$, *Nat. Mater.* **11**, 493 (2012).
- [15] G. Chen, H.-Y. Kee, and Y. B. Kim, Fractionalized Charge Excitations in a Spin Liquid on Partially Filled Pyrochlore Lattices, *Phys. Rev. Lett.* **113**, 197202 (2014).
- [16] J.-P. Lv, G. Chen, Y. Deng, and Z. Y. Meng, Coulomb Liquid Phases of Bosonic Cluster Mott Insulators on a Pyrochlore Lattice, *Phys. Rev. Lett.* **115**, 037202 (2015).
- [17] D. I. Khomskii and S. V. Streltsov, Orbital Effects in Solids: Basics, Recent Progress, and Opportunities, *Chem. Rev.* **121**, 2992 (2021).
- [18] T. Dey, M. Majumder, J. C. Orain, A. Senyshyn, M. Prinz-Zwick, S. Bachus, Y. Tokiwa, F. Bert, P. Khuntia, N. Büttgen, A. A. Tsirlin, and P. Gegenwart, Persistent low-temperature spin dynamics in the mixed-valence iridate $\text{Ba}_3\text{InIr}_2\text{O}_9$, *Phys. Rev. B* **96**, 174411 (2017).
- [19] Y. Li, A. A. Tsirlin, T. Dey, P. Gegenwart, R. Valentí, and S. M. Winter, Soft and anisotropic local moments in $4d$ and $5d$ mixed-valence M_2O_9 dimers, *Phys. Rev. B* **102**, 235142 (2020).
- [20] A. Revelli, M. Moretti Sala, G. Monaco, M. Magnaterra, J. Attig, L. Peterlini, T. Dey, A. A. Tsirlin, P. Gegenwart, T. Fröhlich, M. Braden, C. Grams, J. Hemberger, P. Becker, P. H. M. van Loosdrecht, D. I. Khomskii, J. van den Brink, M. Hermanns, and M. Grüninger, Quasimolecular electronic structure of the spin-liquid candidate $\text{Ba}_3\text{InIr}_2\text{O}_9$, *Phys. Rev. B* **106**, 155107 (2022).
- [21] H. Barz, New ferromagnetic molybdenum spinels, *Mater. Res. Bull.* **8**, 983 (1973).
- [22] H. Yaich, J. Jegaden, M. Potel, M. Sergent, A. Rastogi, and R. Tournier, Nouveaux chalcogénures et chalcologénures à clusters tétraédriques Nb_4 ou Ta_4 , *J. Less-Comm. Met.* **102**, 9 (1984).
- [23] R. Pocha, D. Johrendt, B. Ni, and M. M. Abd-Elmeguid, Crystal Structures, Electronic Properties, and Pressure-Induced Superconductivity of the Tetrahedral Cluster Compounds GaNb_4S_8 , GaNb_4Se_8 , and GaTa_4Se_8 , *J. Am. Chem. Soc.* **127**, 8732 (2005).
- [24] K. Geirhos, S. Reschke, S. Ghara, S. Krohns, P. Lunkenheimer, and I. Kézsmárki, Optical, Dielectric, and Magneto-electric Properties of Ferroelectric and Antiferroelectric Lacunar Spinels, *Phys. status solidi (b)* **259**, 2100160 (2022).
- [25] H.-S. Kim, J. Im, M. Han, and H. Jin, Spin-orbital entangled molecular j_{eff} states in lacunar spinel compounds, *Nat. Commun.* **5**, 3988 (2014).
- [26] M. Y. Jeong, S. H. Chang, B. H. Kim, J.-H. Sim, A. Said, D. Casa, T. Gog, E. Janod, L. Cario, S. Yunoki, *et al.*, Direct experimental observation of the molecular $J_{\text{eff}} = 3/2$ ground state in the lacunar spinel GaTa_4Se_8 , *Nat. Commun.* **8**, 782 (2017).
- [27] D. Johrendt, Crystal and Electronic Structure of the Tetrahedral V_4 Cluster Compounds GeV_4Q_8 ($\text{Q} = \text{S}, \text{Se}$), *Z. anorg. allg.*

- Chem. **624**, 952 (1998).
- [28] S. A. Nikolaev and I. V. Solov'yev, Microscopic theory of electric polarization induced by skyrmionic order in GaV_4S_8 , Phys. Rev. B **99**, 100401(R) (2019).
- [29] H. Lee, M. Y. Jeong, J.-H. Sim, H. Yoon, S. Ryee, and M. J. Han, Charge density functional plus U calculation of lacunar spinel GaM_4Se_8 ($M = \text{Nb, Mo, Ta, and W}$), Europhys. Lett. **125**, 47005 (2019).
- [30] H.-S. Kim, K. Haule, and D. Vanderbilt, Molecular Mott state in the deficient spinel GaV_4S_8 , Phys. Rev. B **102**, 081105(R) (2020).
- [31] L. Hozoi, M. S. Eldeeb, and U. K. Röbber, V_4 tetrahedral units in AV_4X_8 lacunar spinels: Near degeneracy, charge fluctuations, and configurational mixing within a valence space of up to 21 d orbitals, Phys. Rev. Res. **2**, 022017(R) (2020).
- [32] T. Petersen, P. Bhattacharyya, U. K. Röbber, and L. Hozoi, Resonating holes vs molecular spin-orbit coupled states in group-5 lacunar spinels, Nat. Commun. **14**, 5218 (2023).
- [33] I. Kézsmárki, S. Bordács, P. Milde, E. Neuber, L. M. Eng, J. S. White, H. M. Rønnow, C. D. Dewhurst, M. Mochizuki, K. Yanai, H. Nakamura, D. Ehlers, V. Tsurkan, and A. Loidl, Néel-type skyrmion lattice with confined orientation in the polar magnetic semiconductor GaV_4S_8 , Nat. Mater. **14**, 1116 (2015).
- [34] E. Ruff, S. Widmann, P. Lunkenheimer, V. Tsurkan, I. K. S. Bordács, and A. Loidl, Multiferroicity and skyrmions carrying electric polarization in GaV_4S_8 , Sci. Adv. **1**, e15009 (2015).
- [35] S. Bordács, A. Butykai, B. G. Szigeti, J. S. White, R. Cubitt, A. O. Leonov, S. Widmann, D. Ehlers, H.-A. K. von Nidda, V. Tsurkan, A. Loidl, and I. Kézsmárki, Equilibrium Skyrmion Lattice Ground State in a Polar Easy-plane Magnet, Sci. Rep. **7**, 7584 (2017).
- [36] A. Butykai, K. Geirhos, D. Szaller, L. F. Kiss, L. Balogh, M. Azhar, M. Garst, L. DeBeer-Schmitt, T. Waki, Y. Tabata, H. Nakamura, I. Kézsmárki, and S. Bordács, Squeezing the periodicity of Néel-type magnetic modulations by enhanced Dzyaloshinskii-Moriya interaction of $4d$ electrons, npj Quant. Materials **7**, 26 (2022).
- [37] S. Ghara, K. Geirhos, L. Kuerten, P. Lunkenheimer, V. Tsurkan, M. Fiebig, and I. Kézsmárki, Giant conductivity of mobile domain walls, Nat. Comm. **12**, 3975 (2021).
- [38] K. Geirhos, J. Langmann, L. Prodan, A. A. Tsirlin, A. Misul, G. Eickerling, A. Jesche, V. Tsurkan, P. Lunkenheimer, W. Scherer, and I. Kézsmárki, Cooperative Cluster Jahn-Teller Effect as a Possible Route to Antiferroelectricity, Phys. Rev. Lett. **126**, 187601 (2021).
- [39] L. Puntigam, M. Althaler, S. Ghara, L. Prodan, V. Tsurkan, S. Krohns, I. Kézsmárki, and D. M. Evans, Strain Driven Conducting Domain Walls in a Mott Insulator, Adv. Electron.Mater. **8**, 2200366 (2022).
- [40] K. Geirhos, B. Gross, B. G. Szigeti, A. Mehlin, S. Philipp, J. S. White, R. Cubitt, S. Widmann, S. Ghara, P. Lunkenheimer, V. Tsurkan, E. Neuber, D. Ivaneyko, P. Milde, L. M. Eng, A. O. Leonov, S. Bordács, M. Poggio, and I. Kézsmárki, Macroscopic manifestation of domain-wall magnetism and magnetoelectric effect in a Néel-type skyrmion host, npj Quantum Mater. **5**, 44 (2020).
- [41] M. J. Park, G. Sim, M. Y. Jeong, A. Mishra, M. J. Han, and S. Lee, Pressure-induced topological superconductivity in the spin-orbit Mott insulator GaTa_4Se_8 , npj Quantum Mater. **5**, 41 (2020).
- [42] H. Deng, J. Zhang, M. Y. Jeong, D. Wang, Q. Hu, S. Zhang, R. Sereika, T. Nakagawa, B. Chen, X. Yin, H. Xiao, X. Hong, J. Ren, M. J. Han, J. Chang, H. Weng, Y. Ding, H.-Q. Lin, and H.-K. Mao, Metallization of Quantum Material GaTa_4Se_8 at High Pressure, J. Phys. Chem. Lett. **12**, 5601 (2021).
- [43] M. Y. Jeong, S. H. Chang, H. J. Lee, J.-H. Sim, K. J. Lee, E. Janod, L. Cario, A. Said, W. Bi, P. Werner, A. Go, J. Kim, and M. J. Han, $J_{\text{eff}} = \frac{3}{2}$ metallic phase and unconventional superconductivity in GaTa_4Se_8 , Phys. Rev. B **103**, L081112 (2021).
- [44] V. Guiot, L. Cario, E. Janod, B. Corraze, V. Ta Phuoc, M. Rozenberg, P. Stoliar, T. Cren, and D. Roditchev, Avalanche breakdown in $\text{GaTa}_4\text{Se}_{8-x}\text{Te}_x$ narrow-gap Mott insulators, Nat. Commun. **4**, 1722 (2013).
- [45] Y. Ma and M. Blume, Interference of fluorescence x-rays and coherent excitation of core levels, Rev. Sci. Instrum. **66**, 1543 (1995).
- [46] A. Revelli, M. Moretti Sala, G. Monaco, P. Becker, L. Bohatý, M. Hermanns, T. C. Koethe, T. Fröhlich, P. Warzanowski, T. Lorenz, S. V. Streltsov, P. H. M. van Loosdrecht, D. I. Khomskii, J. van den Brink, and M. Grüninger, Resonant inelastic x-ray incarnation of Young's double-slit experiment, Sci. Adv. **5**, eaav4020 (2019).
- [47] M. Magnaterra, M. Moretti Sala, G. Monaco, P. Becker, M. Hermanns, P. Warzanowski, T. Lorenz, D. I. Khomskii, P. H. M. van Loosdrecht, J. van den Brink, and M. Grüninger, RIXS interferometry and the role of disorder in the quantum magnet $\text{Ba}_3\text{Ti}_{3-x}\text{Ir}_x\text{O}_9$, Phys. Rev. Res. **5**, 013167 (2023).
- [48] A. Revelli, M. Moretti Sala, G. Monaco, C. Hickey, P. Becker, F. Freund, A. Jesche, P. Gegenwart, T. Eschmann, F. L. Buessen, S. Trebst, P. H. M. van Loosdrecht, J. van den Brink, and M. Grüninger, Fingerprints of Kitaev physics in the magnetic excitations of honeycomb iridates, Phys. Rev. Res. **2**, 043094 (2020).
- [49] M. Winkler, L. Prodan, V. Tsurkan, P. Lunkenheimer, and I. Kézsmárki, Antipolar transitions in GaNb_4Se_8 and GaTa_4Se_8 , Phys. Rev. B **106**, 115146 (2022).
- [50] V. Ta Phuoc, C. Vaju, B. Corraze, R. Sopracase, A. Perucchi, C. Marini, P. Postorino, M. Chligui, S. Lupi, E. Janod, and L. Cario, Optical Conductivity Measurements of GaTa_4Se_8 Under High Pressure: Evidence of a Bandwidth-Controlled Insulator-to-Metal Mott Transition, Phys. Rev. Lett. **110**, 037401 (2013).
- [51] S. Reschke, F. Meggle, F. Mayr, V. Tsurkan, L. Prodan, H. Nakamura, J. Deisenhofer, C. A. Kuntscher, and I. Kézsmárki, Lattice dynamics and electronic excitations in a large family of lacunar spinels with a breathing pyrochlore lattice structure, Phys. Rev. B **101**, 075118 (2020).
- [52] S. Kawamoto, T. Higo, T. Tomita, S. Suzuki, Z. M. Tian, K. Mochizuki, A. Matsuo, K. Kindo, and S. Nakatsuji, Frustrated magnetism in a Mott insulator based on a transition metal chalcogenide, J. Phys: Conf. Series **683**, 012025 (2016).
- [53] T. Petersen, L. Prodan, V. Tsurkan, H.-A. Krug von Nidda, I. Kézsmárki, U. K. Röbber, and L. Hozoi, How Correlations and Spin-Orbit Coupling Work within Extended Orbitals of Transition-Metal Tetrahedra of $4d/5d$ Lacunar Spinel, J. Phys. Chem. Lett. **13**, 1681 (2022).
- [54] H. Ishikawa, T. Yajima, A. Matsuo, Y. Ihara, and K. Kindo, Nonmagnetic Ground States and a Possible Quadrupolar Phase in $4d$ and $5d$ Lacunar Spinel Selenides GaM_4Se_8 ($M = \text{Nb, Ta}$), Phys. Rev. Lett. **124**, 227202 (2020).
- [55] S. Jakob, *Strukturen, Magnetismus und Phasenumwandlungen der Mott-Isolatoren $\text{Ga}(M_{4-x}M'_x)Q_8$ und $(M_{4-x}M'_x)Q_4I_4$ ($M, M' = \text{Mo, Nb, Ta}$; $Q = \text{S, Se}$; $x = 0 - 4$)*, Ph.D. thesis, Ludwig-Maximilians-Universität München (2007).
- [56] T.-H. Yang, S. Kawamoto, T. Higo, S. G. Wang, M. B. Stone, J. Neufeind, J. P. C. Ruff, A. M. M. Abeykoon, Y.-S. Chen, S. Nakatsuji, and K. W. Plumb, Bond ordering and

- molecular spin-orbital fluctuations in the cluster Mott insulator GaTa_4Se_8 , *Phys. Rev. Res.* **4**, 033123 (2022).
- [57] Y. Shvyd'ko, J. Hill, C. Burns, D. Coburn, B. Brajuskovic, D. Casa, K. Goetze, T. Gog, R. Khachatryan, J.-H. Kim, C. Kodituwakku, M. Ramanathan, T. Roberts, A. Said, H. Sinn, D. Shu, S. Stoupin, M. Upton, M. Wiczorek, and H. Yavas, MERIX—Next generation medium energy resolution inelastic X-ray scattering instrument at the APS, *J. Electron Spectrosc. Relat. Phenom.* **188**, 140 (2013).
- [58] M. Minola, G. Dellea, H. Gretarsson, Y. Y. Peng, Y. Lu, J. Porras, T. Loew, F. Yakhou, N. B. Brookes, Y. B. Huang, J. Pellicciari, T. Schmitt, G. Ghiringhelli, B. Keimer, L. Braicovich, and M. Le Tacon, Collective nature of spin excitations in superconducting cuprates probed by resonant inelastic x-ray scattering, *Phys. Rev. Lett.* **114**, 217003 (2015).
- [59] The *Supplementary Information* discusses spin-orbit coupling on the cluster, the role of non-cubic distortions, and the cluster calculations in the interacting many-body picture, .
- [60] L. J. P. Ament, G. Khaliullin, and J. van den Brink, Theory of resonant inelastic x-ray scattering in iridium oxide compounds: Probing spin-orbit-entangled ground states and excitations, *Phys. Rev. B* **84**, 020403(R) (2011).
- [61] L. J. P. Ament, M. van Veenendaal, T. P. Devereaux, J. P. Hill, and J. van den Brink, Resonant inelastic x-ray scattering studies of elementary excitations, *Rev. Mod. Phys.* **83**, 705 (2011).
- [62] M. W. Haverkort, Quanta for core level spectroscopy - excitons, resonances and band excitations in time and frequency domain, *J. Phys. Conf. Ser.* **712**, 012001 (2016).
- [63] H. Ishikawa, T. Takayama, R. K. Kremer, J. Nuss, R. Dinnebier, K. Kitagawa, K. Ishii, and H. Takagi, Ordering of hidden multipoles in spin-orbit entangled $5d^1$ Ta chlorides, *Phys. Rev. B* **100**, 045142 (2019).
- [64] W. A. Harrison, *Electronic Structure and the Properties of Solids: The Physics of the Chemical Bond* (Dover, 1989).
- [65] S. Sugano, Y. Tanabe, and H. Kamimura, *Multiplets of Transition-Metal Ions in Crystals* (Academic, New York, 1970).

SUPPLEMENTARY INFORMATION

I. SPIN-ORBIT COUPLING ON THE CLUSTER

Before addressing the tetrahedral cluster, we start by considering a single site in cubic symmetry with the three t_{2g} orbitals $X = yz$, $Y = zx$, and $Z = xy$. Applying spin-orbit coupling $H_{\text{SOC}} = \zeta \vec{l} \vec{s}$ to the single electron configuration t_{2g}^1 couples $|X \uparrow\rangle$, $|Y \uparrow\rangle$, and $|Z \downarrow\rangle$ as well as $|X \downarrow\rangle$, $|Y \downarrow\rangle$, and $|Z \uparrow\rangle$ [65], which is described by the two Hamiltonians

$$H_{X\uparrow, Y\uparrow, Z\downarrow} = \begin{pmatrix} 0 & i & -1 \\ -i & 0 & i \\ -1 & -i & 0 \end{pmatrix} \frac{\zeta}{2} \quad (5)$$

$$H_{X\downarrow, Y\downarrow, Z\uparrow} = \begin{pmatrix} 0 & -i & 1 \\ i & 0 & i \\ 1 & -i & 0 \end{pmatrix} \frac{\zeta}{2} \quad (6)$$

where the indices denote the basis states. Altogether, this yields a $j = 3/2$ ground state and a $j = 1/2$ excited state at $3/2 \zeta$.

For the four Ta sites of a tetrahedron, we consider hopping t_σ and t_π between the $4 \times 3 t_{2g}$ orbitals as well as spin-orbit coupling on each of the four sites. Then we transform to the quasimolecular basis states of the hopping Hamiltonian, see Fig. 3a) of the main text. For the single-particle model, we project spin-orbit coupling to the quasimolecular t_2 states. (For comparison, we also consider the case of spin-orbit coupling acting on all states. These exceptions are clearly marked in the main text.) This is a reasonable approximation as long as the energy difference between the quasimolecular states is large. In spirit, it is analogous to neglecting the e_g orbitals in the discussion of a single site. We find a Hamiltonian that is equivalent to the single-site case,

$$H_{X_{\text{tet}}\uparrow, Y_{\text{tet}}\uparrow, Z_{\text{tet}}\downarrow} = \begin{pmatrix} 0 & i & -1 \\ -i & 0 & i \\ -1 & -i & 0 \end{pmatrix} \frac{\zeta}{2} \frac{\alpha^2 - 1}{\alpha^2 + 2} \quad (7)$$

$$H_{X_{\text{tet}}\downarrow, Y_{\text{tet}}\downarrow, Z_{\text{tet}}\uparrow} = \begin{pmatrix} 0 & -i & 1 \\ i & 0 & i \\ 1 & -i & 0 \end{pmatrix} \frac{\zeta}{2} \frac{\alpha^2 - 1}{\alpha^2 + 2} \quad (8)$$

where $Z_{\text{tet}} = t_2(xy)$ is defined in Eq. (3) of the main text. Equivalent expressions hold for X_{tet} and Y_{tet} . Compared to a single site, the energy scale is renormalized by α , see Fig. 3b). The normalization factor approaches 1 in the limit $\alpha = \infty$.

II. EFFECT OF NON-CUBIC DISTORTIONS

In cubic symmetry, all Ta-Ta edges of the regular tetrahedron are of equal length $d = 3.0 \text{ \AA}$. However, the symmetry is lower than cubic below $T_{ms} = 53 \text{ K}$. Furthermore, recent x-ray and neutron results on the pair distribution function [56] point to dynamical local distortions up to temperatures far above T_{ms} . These dynamical distortions are of similar size as the

static distortions at low temperature. RIXS averages over different orientations of the dynamical distortions above T_{ms} and different domains below T_{ms} . Even within a single domain, different tetrahedra within the unit cell show different orientations [56]. For a single tetrahedron, we approximate the distorted case by three short and three long bonds with $3.0 \pm 0.04 \text{ \AA}$, where the long bonds meet at one Ta site [56]. We implement such a trigonal distortion of the tetrahedron via the size of σ -type hopping, for which we assume $t_\sigma \mp \Delta/2$. With $t_\sigma \propto 1/d^5$ [64], we estimate $\Delta/t_\sigma \approx 0.13$. Below we use $\Delta = 0.2 \text{ eV}$, which somewhat overestimates the effect of a trigonal distortion.

As in the cubic case, we employ the single-particle picture and first calculate the eigenstates of the hopping Hamiltonian for a single, distorted tetrahedron. Then we apply spin-orbit coupling within the t_2^1 states. The distortion splits the $J_{\text{tet}} = 3/2$ quartet into two doublets, in close analogy to the single-site case. We calculate RIXS for the four equivalent orientations of the distortion and finally average over the four curves. Figure 5 shows the result for peak A along $(7.35 \ 7.35 \ l)$ for $\Delta = 0.2 \text{ eV}$ and $\alpha = 2.4$. We find clear differences for different orientations of the distortion. RIXS thus would be sensitive to the distortion if a single orientation of the distortion could be measured. However, the average over the four distorted results is very close to the RIXS response of the undistorted case. This is a plausible explanation for our RIXS data being very similar at 20 K and 100 K and validates the description of the data in terms of a cubic model.

Peak B corresponds to excitations from e to $J_{\text{tet}} = 3/2$ states. The $J_{\text{tet}} = 3/2$ quartet contains states with $J^z = \pm 1/2$ and $J^z = \pm 3/2$, and these show a different \mathbf{q} dependence, see Fig. 6. In particular a nearly \mathbf{q} -independent behavior is observed for $\alpha \approx 1.1$ for $J^z = \pm 1/2$ but for $\alpha \approx 3$ for $J^z = \pm 3/2$. The trigonal distortion considered above mixes these two states with equal weight, and hence has little effect on the \mathbf{q} dependence. However, a distortion of lower symmetry may cause preferential occupation of, e.g., $J^z = \pm 1/2$ in the ground state, which will partially block the corresponding contribution. In this case, a \mathbf{q} -independent behavior is ex-

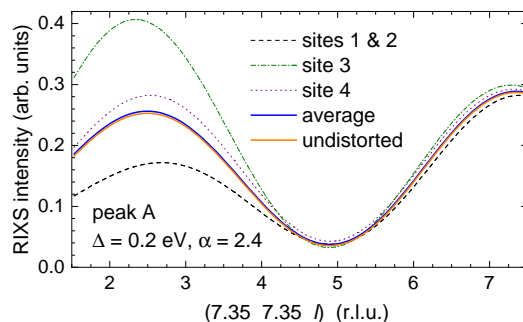


FIG. 5. RIXS intensity of peak A for \mathbf{q} along $(7.35 \ 7.35 \ l)$ for a distorted tetrahedron with $\Delta = 0.2 \text{ eV}$ and $\alpha = 2.4$. For this \mathbf{q} direction, the results for distortions with either site 1 or 2 as unique site are identical. The average over the four different orientations of the distortion (solid blue line) is hard to distinguish from the undistorted case (solid orange line).

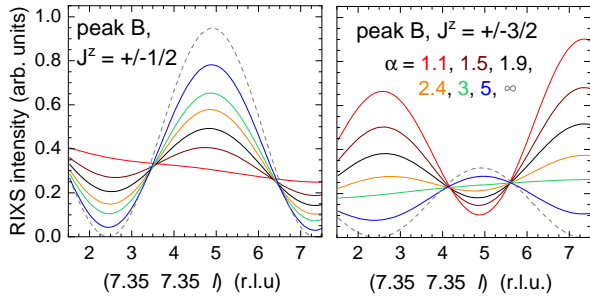


FIG. 6. The α dependence of the RIXS intensities of the two different contributions to peak B. Left (right): Excitations from an e orbital to $J_{\text{tet}} = 3/2$ with $J^z = \pm 1/2$ ($\pm 3/2$).

pected for a larger value of α up to $\alpha = 2.2$. It is plausible that such a low-symmetry distortion may describe the behavior of peaks A and B for the same value of α .

III. ELECTRON-ELECTRON INTERACTIONS

Beyond the calculations within the single-particle model, we also performed many-body cluster calculations using Quany [62]. For the seven t_{2g} electrons on a Ta_4 tetrahedron, we consider the model Hamiltonian $H = H_t + H_\zeta + H_{e-e}$ that takes into account hopping t_σ and t_π , spin-orbit coupling ζ , and electron-electron interactions, i.e., on-site Coulomb repulsion U and Hund's coupling J_H . We first diagonalize H_t and then consider the lower nine (a_1 , e , t_2 , and t_1) out of 12 quasimolecular orbitals, see Fig. 3a) of the main text.

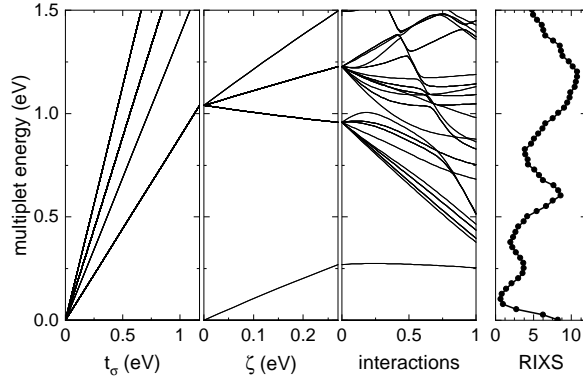


FIG. 7. Excitation energies of a single Ta_4 tetrahedron (left) compared to a RIXS spectrum (right). The plot focuses on the low-energy sector, in particular on intra- t_2 and e -to- t_2 excitations. First panel: effect of hopping t_σ for fixed $|t_\sigma/t_\pi| \approx 2.6$, i.e., $\alpha = 2.9$. Beyond the $a_1^2 e^4 t_2^2$ ground state manifold at zero energy it shows, with increasing energy, the states $a_1^2 e^3 t_2^2$, $a_1^2 e^4 t_2^0 t_1^1$, $a_1^2 e^3 t_2^3$, and $a_1^2 e^3 t_2^1 t_1^1$. Second panel: finite ζ lifts the degeneracy of the $a_1^2 e^3 t_2^2$ states at about 1 eV while the $a_1^2 e^4 t_2^2$ ground state is split into $J_{\text{tet}} = 3/2$ and $1/2$ with an excitation energy of about ζ . Third panel: Electron-electron interactions are necessary to correctly describe the excitation energies of peaks B and C. The scale 0 to 1 encodes the linear increase from $J_H = U = 0$ to $J_H = 0.4$ eV and $U = 1.75$ eV.

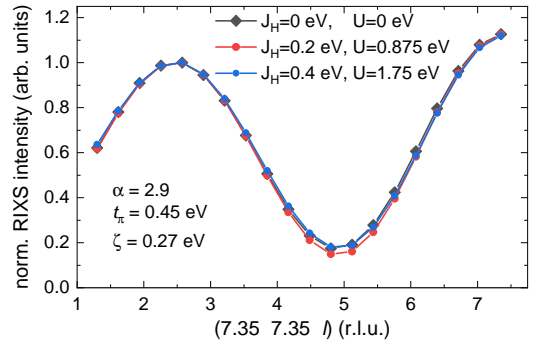


FIG. 8. Effect of electron-electron interactions on the \mathbf{q} dependence of the normalized RIXS intensity of peak A along $(7.35 \ 7.35 \ l)$ for $\alpha = 2.9$.

Taking into account electron-electron interactions is in particular necessary in order to correctly reproduce the excitation energies of peaks B and C as well as the width of peak C. Figure 7 shows the low-energy excitation energies of a Ta_4 tetrahedron, in particular for intra- t_2 and e -to- t_2 excitations. The first panel on the left depicts the effect of hopping t_σ and t_π for a fixed ratio $|t_\sigma/t_\pi| \approx 2.6$, i.e., $\alpha = 2.9$, while the second panel introduces spin-orbit coupling ζ . Both panels employ $H_{e-e} = 0$, i.e., the non-interacting scenario. For $\zeta = 0$, the ground state configuration is within the $a_1^2 e^4 t_2^2$ manifold, while the lowest excited states correspond to $a_1^2 e^3 t_2^2$. Finite ζ yields a $J_{\text{tet}} = 3/2$ ground state and a $J_{\text{tet}} = 1/2$ doublet at an energy of roughly ζ , i.e., the excitation energy is reduced from the expectation 1.5ζ for $\alpha = \infty$, see Fig. 3b) of the main text. Figure 3b) also shows that the renormalization is slightly different compared to our single-particle calculations and that the normalization depends on the set of orbitals to which spin-orbit coupling is restricted. At higher energy, ζ splits the $a_1^2 e^3 t_2^2$ manifold into three energy levels that, in the absence of electron-electron interactions, can be distinguished according to the occupation of the t_2 states: $J_{3/2}^2$, $J_{3/2}^1 J_{1/2}^1$, and $J_{1/2}^2$. Note that the latter state cannot be reached from a $J_{3/2}^1$ ground state in a single-particle scenario. The two lower branches hence correspond to peaks B and C. Electron-electron interactions cause a fanning out of energies for the $a_1^2 e^3 t_2^2$ states but have little effect on the low-energy $a_1^2 e^4 t_2^2$ states, i.e., $J_{\text{tet}} = 3/2$ and $1/2$. Based on the RIXS peak energies and the \mathbf{q} dependence, we employ $\alpha = 2.9$, $t_\pi = 0.45$ eV, $t_\sigma \approx 1.17$ eV, $\zeta = 0.27$ eV, $U = 1.75$ eV, and $J_H = 0.4$ eV. These parameters have also been used for Fig. 3b) of the main text, where α has been changed by varying t_σ .

The single-particle model offers a very good description of peak A, the excitation from $J_{\text{tet}} = 3/2$ to $1/2$ within the $a_1^2 e^4 t_2^2$ manifold. This result is stable against the addition of electron-electron interactions. For $\alpha = 2.9$, Fig. 8 compares the \mathbf{q} -dependent intensity of peak A along $(7.35 \ 7.35 \ l)$ for vanishing, intermediate, and sizable electron-electron interactions. For all three curves, spin-orbit coupling acts within the lower nine quasimolecular orbitals, i.e., a_1 , e , t_2 , and t_1 . The behavior is very similar, and we conclude that electron-electron interactions have only a minor effect on peak A.